CORE
Metadata, citation and similar papers at core.ac.uk
Provided by Elsevier - Publisher Connector

Evolving Technology

Time-resolved three-dimensional magnetic resonance velocity mapping of aortic flow in healthy volunteers and patients after valve-sparing aortic root replacement

Michael Markl, PhD,[a] Mary T. Draney, PhD,[b] D. Craig Miller, MD,[c] Jonathan M. Levin, MD,[a] Eric E. Williamson, MD,[a] Norbert J. Pelc, ScD,[a] David H. Liang, MD, PhD,[d] and Robert J. Herfkens, MD[a]

Objective: To provide more complete characterization of ascending aortic blood flow, including vortex formation behind the valve cusps, in healthy subjects and patients after valve-sparing aortic root replacement (David reimplantation).

Methods: Time-resolved 3-dimensional magnetic resonance imaging velocity mapping was performed to analyze pulsatile blood flow by using encoded 3-directional vector fields in the thoracic aortas of 10 volunteers and 12 patients after David reimplantation using a cylindrical tube graft (T. David I) and two versions of neosinus recreation (T. David-V and T. David-V-S_{mod}). Aortic flow was evaluated by using 3-dimensional time-resolved particle traces and velocity vector fields reformatted onto 2-dimensional planes. Semiquantitative data were derived by using a blinded grading system (0-3: 0, none; 1, minimal; 2, medium; 3, prominent) to analyze the systolic vortex formation behind the cusps, as well as retrograde and helical flow in the ascending aorta.

Results: Systolic vortices were seen in both coronary sinuses of all volunteers (greater in the left sinus [2.5 ± 0.5] than the right [1.8 ± 0.8]) but in only 4 of 10 noncoronary sinuses (0.7 ± 0.9). Comparable coronary vortices were detected in all operated patients. Vorticity was minimal in the noncoronary cusp in T. David-I repairs (0.7 ± 0.7) but was prominent in T. David-V noncoronary graft pseudosinuses (1.5 ± 0.6; $P = .035$). Retrograde flow ($P = .001$) and helicity ($P = .028$) were found in all patients but were not distinguishable from normal values in the T. David-V-S_{mod} patients.

Conclusions: Coronary cusp vorticity was preserved after David reimplantation, regardless of neosinus creation. Increased retrograde flow and helicity were more prominent in T. David-V patients. These novel magnetic resonance imaging methods can assess the clinical implications of altered aortic flow dynamics in patients undergoing various types of valve-sparing aortic root replacement.

ET

From the Department of Radiology,[a] Department of Mechanical Engineering,[b] Department of Cardiothoracic Surgery,[c] and Division of Cardiovascular Medicine,[d] Stanford University, Stanford, Calif.

Supported by National Institutes of Health grants R01 HL46347 and NIH P41 RR09784, Deutsche Forschungsgemeinschaft fellowship MA2383/1-1, the Kyle Mann Fund (Stanford University), and The Lucas Foundation.

Read at the Thirtieth Annual Meeting of The Western Thoracic Surgical Association, Maui, Hawaii, June 23-26, 2004.

Received for publication April 27, 2004; revisions received Aug 11, 2004; accepted for publication Aug 20, 2004.

Address for reprints: Robert J. Herfkens MD, Stanford University, Department of Radiology, Lucas MRI/S Center, P263, Palo Alto, CA 94304 (E-mail: herfkens@stanford.edu).

J Thorac Cardiovasc Surg 2005;130:456-63

0022-5223/$30.00

Copyright © 2005 by The American Association for Thoracic Surgery

doi:10.1016/j.jtcvs.2004.08.056

Treatment of aortic root pathology by David reimplantation (valve-sparing root replacement) has been performed since 1988.[1-6] Interest in ascending aortic blood flow dates back to Leonardo da Vinci and was first explored by Bellhouse and Bellhouse[7] in 1968. Although studies investigating the mechanics of reimplanted aortic valves have been reported,[8] only 1 analysis of 3-directional blood

flow in the thoracic aorta and the potential consequences of surgically altered aortic geometry and function has been published.[9]

Magnetic resonance imaging (MRI) provides a noninvasive method for the accurate anatomic characterization of the heart and great vessels within a 3-dimensional (3D) data set.[10,11] In comparison to other imaging modalities, such as computed tomography, the intrinsic sensitivity of MRI with respect to flow and motion offers the unique capability to acquire cardiac-gated and spatially encoded functional information simultaneously with morphologic data in a single study.[12-19] The magnetic resonance (MR) method used simultaneously assessed morphology and blood flow in vivo within a user-defined 3D volume with high spatial resolution (1.2-3 mm). Data were acquired in an electrocardiogram-gated and respiratory-compensated single scan that yielded time-resolved 3-directional pulsatile blood flow throughout the entire thoracic aorta.[20,21] The acquired data set was analyzed by using 3D data reformatting and blood flow visualization tools.[22-24] Three different visualization tools (2-dimensional [2D] vector-fields, 3D streamlines, and 3D particle traces) that use different parts of the information available within the time-resolved 3D data sets were used and focused on flow features near the aortic valve cusps and in the ascending aorta.

The objective of this study was to demonstrate that 3D MR velocity mapping is a reliable technique for the qualitative and quantitative assessment and visualization of blood flow in the ascending aorta and that this technique can portray flow features such as vortex formation in the sinuses of Valsalva or helical aortic flow in volunteers and patients who have undergone valve-sparing aortic root replacement with the T. David reimplantation method. Of particular interest was comparing patients who received different types of valve reimplantation repairs, to analyze the effects of recreating graft neosinuses.

Materials and Methods

Human Subjects

Ten healthy volunteers and 12 patients (7 men and 5 women aged 25-53 years; mean age, 36 years) were evaluated by using time-resolved 3D MR velocity mapping. All patients underwent valve-sparing aortic root replacement with T. David-I (n = 4), T. David-V (n = 5), or T. David-V-S_{mod} (n = 3) reimplantation techniques. The T. David-I method uses a cylindrical tube graft, whereas the other 2 methods create 3 graft neosinuses.[5] The T. David-V-S_{mod} (Stanford modification) procedure used 2 (large proximal and small distal) grafts. One patient (T. David-V) had a bicuspid aortic valve. These studies were performed between 1 week and 92 months (mean, 30 months) after surgery. For comparison, image acquisition and postprocessing tools were evaluated in 10 healthy volunteers (4 men and 6 women; age range, 20-40 years; mean age, 27 years) with no history of cardiovascular disease. All studies were approved by Stanford University's Institutional Review Board, and informed consent was obtained from all subjects.

Data Acquisition

A measurement technique often referred to as phase-contrast MRI, based on the intrinsic velocity sensitivity of the phase of the MR signal to motion, was used to assess blood-flow velocities. These 3D MR velocity mapping techniques were previously described and validated.[20,21]

All experiments were performed on a 1.5-T MR system (Signa CV/I; GE, Milwaukee, Wis) by using a 4-element phased array torso coil. To resolve blood flow and cardiovascular anatomy as a function of cardiac phase (cine imaging), measurements were synchronized to the cardiac cycle by using electrocardiogram gating in combination with real-time parameter updates and were subsequently interpolated to reconstruct 20 images representing different phases of the cardiac cycle. Respiration control was performed by using bellows to estimate the respiratory position for each RR interval; these data were then used to select appropriate phase-encoding amplitudes such that the final data set appeared to be collected during a single respiratory cycle (Figure 1). As a result, the respiratory motion is spread out homogenously across the data matrix. This reduced image artifacts but did create some image blurring.

An oblique sagittal slab was prescribed so that the data set completely covered the ascending and descending thoracic aorta. The following parameters were used for all experiments: fractional echo readout using 70% of the full echo; flip angle α, 15°; bandwidth, $\pm$62.5 kHz, velocity sensitivity, 200 cm/s along all 3 spatial directions; fractional field of view, (300-340 $\times$ 225-240) mm^2; slab thickness, 83.2-96 mm; matrix, 256 $\times$ 144 $\times$ 32; and spatial resolution, (1.17-1.33 $\times$ 1.56-1.67 $\times$ 2.60-3.00) mm^3. Four phase encodes per time frame in combination with 3-directional velocity encoding resulted in a temporal resolution (T_{Res}) that was determined by the time needed to collect 16 k-space lines (T_{Res}= 16TR). T_{Res}, 75.1-80.7 ms, varied among subjects depending on the obliquity of the imaging slab and the echo (TE, 1.84-2.06 ms) and repetition (TR, 4.79-5.04 ms) times. Because 4 phase encodes were collected for each RR interval and the total number of raw data lines is fixed, the total acquisition time is heart rate dependent and ranged from 13.8 to 22.6 minutes.

A routine contrast-enhanced MR angiogram (gadopentate dimeglumine [Magnevist]; 0.3 mmol/kg; injection rate, 2-3 mL/s intravenously) was performed. To improve image quality, the 4-dimensional flow scan was performed immediately after the MR angiogram to enhance the signal-noise ratio given the contrast agent remaining in the blood pool.

A 3D time-resolved steady-state free-precession series was acquired to improve the image quality of the underlying anatomic magnitude images.[25] 3D phase-contrast and 3D time-resolved steady-state free-precession data sets were acquired with identical temporal and spatial resolution to provide equal imaging volumes. The resulting time series of 3D volumes was used to replace the anatomic images in the 3D MR velocity mapping data set to improve image quality and real-time navigation in the time-resolved 3D data set. All patients had a recent transthoracic echocardiogram in which aortic regurgitation (AR) was graded (0, none; 1, minimal; 2, medium; 3, prominent).

ET

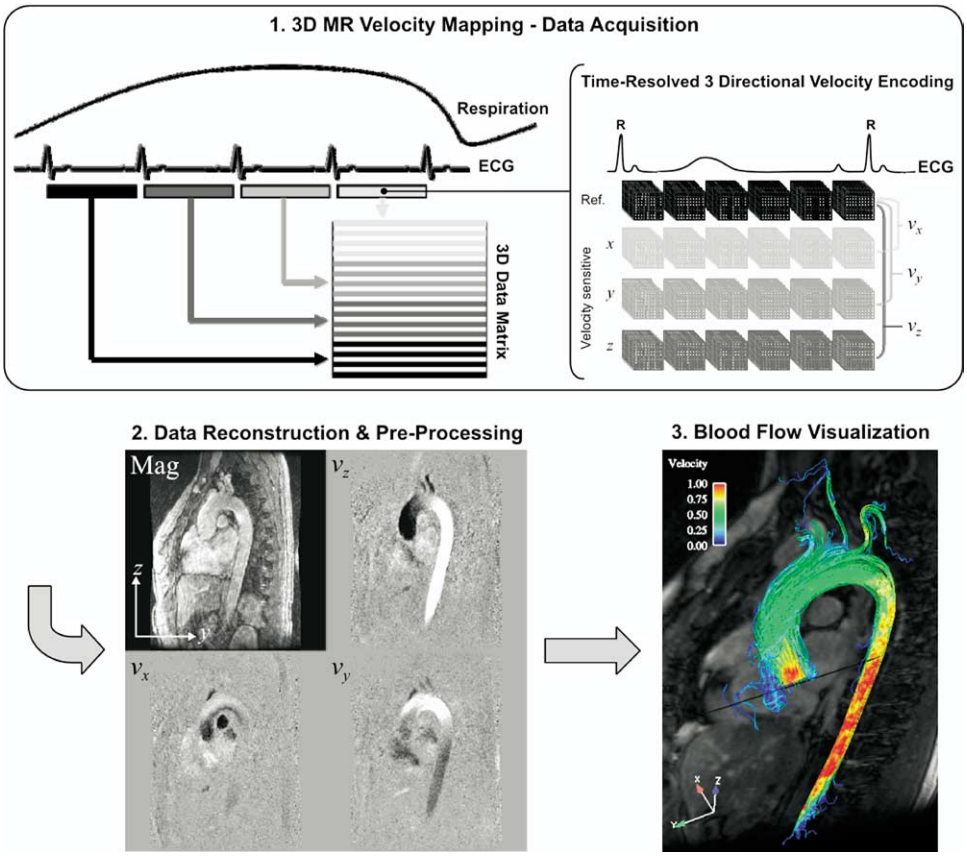

Figure 1. Schematic illustration of data acquisition, data processing, and blood-flow visualization for 3D MR velocity mapping. Top: Electrocardiogram gating and respiratory control (left) and 3-directional velocity encoding (right) for the 3D velocity mapping. After R-wave detection, a real-time estimate of the phase in the respiration cycle was generated and used to adjust the phase-encoding amplitude such that the data matrices mimicked the acquisition in a single respiratory cycle. During each RR interval, a fraction of 4 time-resolved 3D volumes needed for 3-directional velocity encoding was collected, and this process was repeated over consecutive cardiac cycles until all data matrices were completely filled. The 3 spatial components (v_x, v_y, and v_z) of the velocity data were derived by generating phase difference images from the reference (Ref.) and respective velocity-sensitive data set. Bottom left: After retrospective data interpolation, Fourier transform, noise filtering, and eddy current correction, 4 time-resolved 3D data sets were generated reflecting thoracic anatomy (Mag), as well as 3 spatially registered blood-flow velocity components (v_x, v_y, and v_z). The image shown here depicts a single sagittal oblique slice during systole in the acquired 3D volume and 20 reconstructed cardiac phases. Each velocity image represents quantitative Cartesian velocity components in which the grayscale values correspond to the velocity magnitude and direction. Bottom right: blood-flow visualization with 3D streamlines in the thoracic aorta. The individual lines represent traces along the instantaneous velocity vector field in a systolic time frame and are color-coded according to velocity magnitude in meters per second. *ECG,* Electrocardiogram.

ET

Blood-Flow Visualization

After reconstruction and preprocessing (fully automated noise filtering and eddy current correction[26]) of the acquired data, the entire time-resolved 3D MR velocity-mapping data set was loaded into a 3D visualization software package (EnSight; Computational Engineering International, Apex, NC). Blood flow through the ascending aorta was evaluated by using 3-directional velocity vector fields reformatted onto 2D planes transecting the ascending aorta, as well as 3D streamlines and time-resolved 3D particle traces originating at the level of the aortic valve. Velocity vector fields, positioned freely within the imaging volume, were used to analyze blood flow through the aortic valve, as well as vortical flow behind the aortic valve cusps.

To analyze distal ascending aortic retrograde and helical aortic flow, 3D streamlines and particle traces were generated by using equidistant emitter points from a 2D grid of variable size that could be positioned at any spatial location within the 3D data set. In contrast to streamlines, which depict traces along the instantaneous

velocity vector field in a specific time, 3D particle traces use all of the functional information and reflect blood flow throughout the entire cardiac cycle. A schematic representation of this strategy for data acquisition, postprocessing analysis, and 3D blood flow visualization is shown in Figure 1.

Data Analysis

Quantitative analysis of systolic vortex formation behind individual aortic valve cusps (2D velocity vector fields), as well as late systolic and early diastolic retrograde and helical flow in the ascending aorta (time-resolved 3D particle traces), was performed. For all healthy subjects, blood-flow vortices were visualized and evaluated with color-coded velocity vector fields mapped onto different 2D planes transecting the aortic outflow and normal to the valve plane. For each aortic valve cusp, an individual plane was carefully positioned to portray the temporal and spatial evolution of aortic flow surrounding the respective cusp, including the flow in the corresponding sinus. The orientation of the planes was defined by using a systolic image including the opened aortic valve (Figure 2). For patients who underwent the T. David-I procedure, aortic graft neosinuses are nonexistent, and the planes were positioned according to the cusp geometry.

Three images were created for each subject (labeled according to the coronary anatomy: LC, left coronary; RC, right coronary; and NC, noncoronary) that depicted 3-directional systolic blood flow as color-coded velocity vector fields for individual opened valve cusps. Helical and retrograde aortic flow was evaluated by using 3D particle traces that originated at the level of the aortic valve. The presence, orientation, and degree of helical and retrograde flow along the inner wall of the distal ascending aorta were analyzed.

All data sets were presented in a blinded fashion, and the relevant flow features were graded (0, none; 1, minimal; 2, medium; 3, prominent) by 3 experienced radiologists. The variability of average scores is indicated as ±1 standard deviation. Data were compared by using repeated-measures analysis of variance (ANOVA) with a within-subjects factor of reader and a between-subjects factor of diagnosis (normal; type of repair) to determine significant differences. The factorial ANOVA model was used even though the data were an ordinal rather than interval scale, because there is no corresponding nonparametric test that takes advantage of the powerful multireader design.

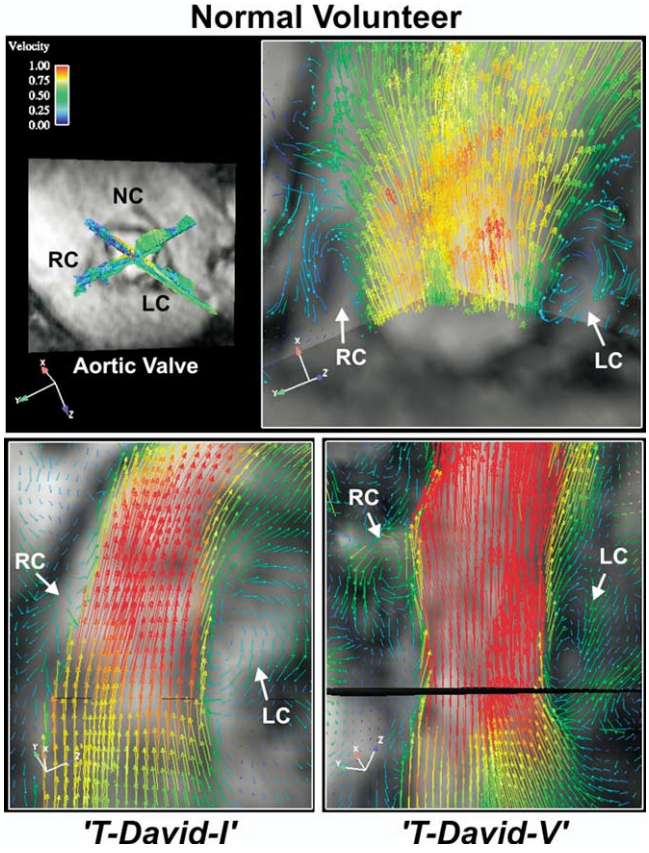

Figure 2. Three-directional velocity vector fields in two 2D planes transecting the ascending aortic flow trace for a healthy volunteer (top) and patients who underwent T. David-I (bottom left) and T. David-V (bottom right) valve-sparing aortic root replacement. The planes were positioned normal to the opened aortic valve (top left) to depict color-coded blood flow velocities near the left coronary *(LC)* and right coronary *(RC)* cusps. Formation of blood-flow vortices is clearly visible in all cases *(arrows)*. Note that the systolic aortic valve anatomy and corresponding 2D plane positions are shown only for the volunteer. Movies corresponding to this figure are available online.

Results

Interobserver agreement was moderate for all flow features evaluated (55%-64%; $\kappa = 0.38$-0.50).

Vortex Formation

Examples of visualization of systolic aortic flow and vortex formation with color-coded velocity vector fields are shown in Figure 2. The images show systolic blood flow velocities behind the 2 coronary cusps for a healthy volunteer (top) and patients who underwent T. David-I (bottom left) and T. David-V (bottom right) aortic root replacement. Vortex formation (arrows) is evident in all 3 cases, even for those with a T. David-I repair without graft neosinuses. Systolic vortical flow was visualized in all 10 volunteers in both coronary sinuses of Valsalva and was most prominent for the LC cusp (score, 2.46 ± 0.53) compared with the RC cusp (score, 1.80 ± 0.83). Vortex formation was less obvious for the NC sinus (score, 0.67 ± 0.93), where vortices could be detected in only 4 of 10 healthy subjects (score, >0.5 where ≥2 observers rated the vortex formation as minimal).

Comparable systolic vortices behind the coronary cusps were detected in all operated patients. Although no neosinuses were recreated in those who underwent the T. David-I procedure, reverse flow and vortex formation behind the 2 opened coronary cusps were clearly visible in all 4 patients

ET

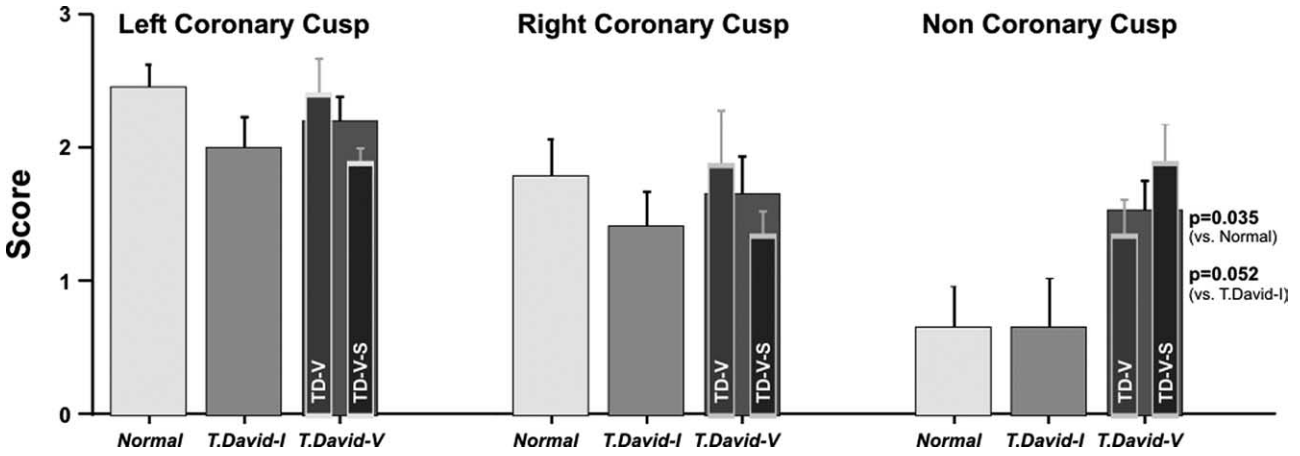

Figure 3. Comparison of average scores for systolic vortex formation as a result of visual image inspection by 3 independent observers. The individual bars represent results for the left, right, and noncoronary cusps. In all cases, comparable systolic vorticity was found for both coronary cusps, whereas noncoronary vortex formation was significantly enhanced for patients who underwent root replacement that included creating graft neosinuses (*TD-V,* T. David-V technique; *TD-V-S,* T. David-V-S_{mod} technique). The error bars indicate ±1 standard deviation.

(score: LC, 2.50 ± 0.58; RC, 2.00 ± 0.47), whereas NC vortex formation was minimal (score: 0.67 ± 0.72). For all 3 cusps, no significant differences in vortex formation were detected between volunteers and T. David-I patients.

Medium to prominent systolic vortical flow in the 2 coronary recreated graft neosinuses was also evident for all T. David-V (score: LC, 2.40 ± 0.60; RC, 1.87 ± 0.93) and T. David-V-S_{mod} (score: LC, 1.89 ± 0.19; RC, 1.33 ± 0.33) patients. For the combined group of patients with either a T. David-V or a T. David-V-S_{mod} reimplantation, however, vortex formation in the recreated NC graft pseudosinus was greater (score: NC, 1.54 ± 0.62; ANOVA: $F_{1,16} = 5.33$; $P = .035$) than in the volunteers. Comparison with T. David-I patients revealed similar vorticity in the 2 coronary sinuses, whereas NC vortex formation was amplified (score: NC, 0.67 ± 0.72; ANOVA: $F_{1,10} = 4.85$), but this was only possibly statistically significant ($P = .052$). Results regarding the quantitative vorticity analysis are summarized in Figure 3.

Aortic Outflow

Echocardiography demonstrated minimal (score: 1) AR in 6 of the operated patients (3 T. David-I, 2 T. David-V, and 1 T. David-V-S_{mod}) and none in the other 6 patients. Analysis of time-resolved 3D particle traces demonstrated right-handed (as viewed from the aortic valve looking cephalad) helical flow in all subjects. At least minimal helicity in the ascending aorta was seen by all 3 observers in all healthy subjects (score: 2.03 ± 0.67).

The analysis of helicity and retrograde flow in the distal ascending aorta is summarized in Tables 1 and 2. For all

TABLE 1. Summary of results of the quantitative analysis of aortic outflow: average score (mean ± standard deviation)

Variable	Volunteers (n = 10)	T. David-I (n = 4)	T. David-V (n = 5)	T. David-V-S_{mod} (n = 3)	All patients (n = 12)
Helix	2.03 ± 0.67	2.58 ± 0.32	2.80 ± 0.45	2.22 ± 0.19	2.58 ± 0.41
Retro flow	1.40 ± 0.54	2.50 ± 0.43	2.27 ± 0.76	2.00 ± 0.00	2.28 ± 0.55

Helix, Helical flow in the ascending aorta; *Retro flow,* retrograde flow in the ascending aorta during late systole and early diastole.

TABLE 2. Summary of results of the quantitative analysis of aortic outflow: group comparisons (analysis of variance)

Variable	T. David-I vs volunteers	T. David-V vs volunteers	T. David-V-S_{mod} vs volunteers	All T. David-V vs volunteers	All patients vs volunteers
Helix	$P = .151$	$P = .040$	$P = .650$	$P = .068$	$P = .028$
Retro flow	$P = .004$	$P = .023$	$P = .089$	$P = .011$	$P = .001$

Helix, Helical flow in the ascending aorta; *Retro flow,* retrograde flow in the ascending aorta during late systole and early diastole.

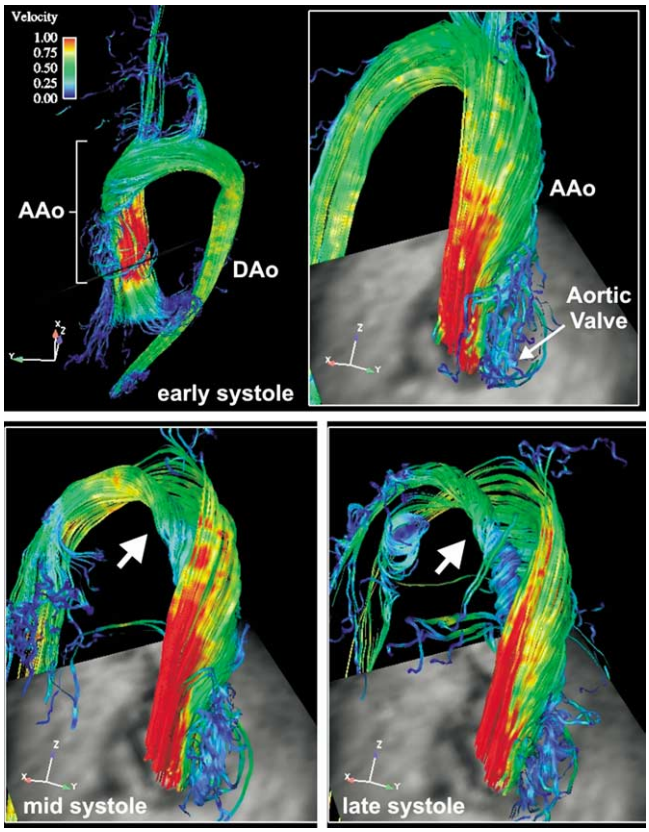

Figure 4. 3D streamlines reflecting systolic blood flow in the thoracic aorta for a patient after T. David-V valve-sparing aortic root replacement. The images on the top right and in the bottom row depict magnified regions including the ascending aorta and the aortic arch, as well as a 2D plane including the aortic valve. Pronounced right-handed helical flow in the ascending aorta *(AAo)* and arch during mid and late systole is evident (*DAo,* Descending aorta). A movie corresponding to this figure is available online.

operated patients, a significant increase in helical flow (score: 2.58 ± 0.41; ANOVA: $F_{1,20} = 5.59$; $P = .028$) was observed compared with volunteers. An example of prominent helical aortic flow for a patient after T. David-V reimplantation is shown in Figure 4. Comparing individual surgical techniques with healthy subjects, helical flow was most prominent for the T. David-V patients (score: 2.80 ± 0.32; ANOVA: $F_{1,13} = 1.20$; $P = .040$). Helical flow in patients with a T. David-V-S_{mod} (score: 2.22 ± 0.19) or a T. David-I (score: 2.58 ± 0.32) procedure, however, was not statistically different from that in volunteers (score= 2.03 ± 0.67).

Minimal late systolic and early diastolic retrograde flow in the distal ascending aorta was observed in all volunteers (score: 1.40 ± 0.54) but was more pronounced in the operated patients (score: 2.28 ± 0.55; ANOVA: $F_{1,20} = 14.20$; $P = .001$). Figure 5 illustrates prominent retrograde flow for a patient who received a T. David-I procedure. Compared with healthy subjects, more distinct retrograde flow was seen in T. David-I patients (score: 2.50 ± 0.43; ANOVA: $F_{1,12} = 14.06$; $P = .004$) than in the T. David-V and T. David-V-S_{mod} patients grouped together (score: 2.17 ± 0.43; ANOVA: $F_{1,16} = 8.25$; $P = .011$).

Discussion

These observations demonstrate that time-resolved 3D velocity mapping is a useful tool for the analysis and visualization of blood-flow characteristics in patients with valve-sparing aortic root replacement. Time-dependent velocities and the anatomy of the entire thoracic aorta were acquired within a single acquisition, thus allowing for qualitative assessment of blood flow in the ascending aorta within a single velocity-encoded 3D data set. In this context, 3D streamlines and particle traces provide a useful analysis of global aortic flow features such as helical and retrograde flow, whereas 2D velocity vector fields are most sensitive for the detection of systolic vortex formation. These tools allow for real-time navigation throughout a prescribed 3D data set during any phase of the cardiac cycle. This enables one to place arbitrarily cut planes throughout the 3D data set without being hindered by the prospective acquisition of traditional 2D phase-contrast MRI.

Results from the healthy volunteers indicated that systolic vortex formation was most prominent in the 2 coronary sinuses of Valsalva, whereas blood flow behind the NC cusp was seen only in 4 of 10 subjects. These observations differ from those recently reported by Kvitting and colleagues,[9] who detected vorticity in all 3 sinuses of 6 healthy subjects. Further, we are puzzled that the Linkoping group[9] saw more

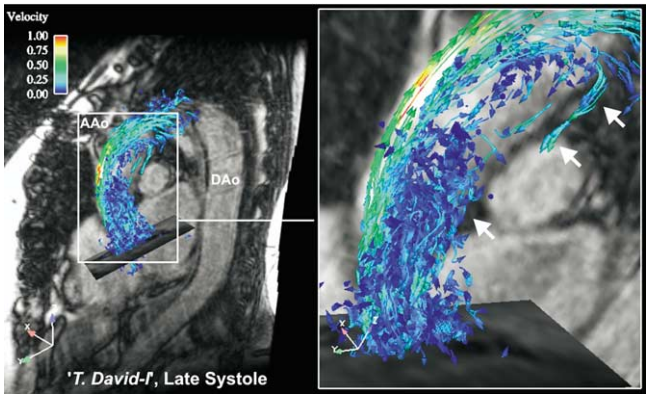

Figure 5. Late systolic 3D particle traces reflecting aortic flow for a patient after T. David-I valve-sparing aortic root replacement. The image on the right shows a magnified region that includes the ascending aorta. Retrograde flow *(white arrows)* along the inner wall of the distal ascending aorta *(AAo)* is clearly visible (*DAo,* Descending aorta). A movie corresponding to this figure is available online.

vorticity in the NC and RC sinuses of volunteers, whereas we observed more vorticity in the RC and LC cusps.

Valve-sparing aortic root replacement (David reimplantation) does not significantly affect the degree of vorticity behind the coronary aortic valve cusps, whether or not graft neosinuses were created. The patients who underwent T. David-V and T. David-V-S_{mod} procedures exhibited readily detectable systolic vortex formation (with significantly more vortex formation in the NC sinus). Even patients who received the T. David-I procedure demonstrated substantial reverse flow and vorticity behind the opened coronary valve cusps. Therefore, it can be postulated that systolic vortex formation is not predominantly a consequence of the mechanical and geometrical properties of the sinuses of Valsalva but is more related to aortic blood flow and associated hemodynamics (eg, pressure differences across the aortic cusps). The recent MRI report from Linkoping[9] did not observe any vorticity in 2 T. David-I patients, whereas such was seen in all 4 of our T. David-I patients; this disparity may be explained in part by differences in the acquisition voxel volume (16 mm^3 in their images vs 4.7-6.7 mm^3), anisotropic voxel orientation, or other differences in image-acquisition methods. Further, the Linkoping group studied only streamline visualizations, whereas we used all 3 techniques (2D velocity vector fields, 3D streamlines, and 3D particle traces), which yielded similar findings with respect to vorticity. Although vortex formation was enhanced by the surgical creation of graft neosinuses in the T. David-V patients, normal vorticity was preserved even without sinus creation in the graft. In operated patients, considerably enhanced helical flow patterns could be identified with 3D particle traces in the distal ascending aorta, particularly in the T. David-V subgroup. Further studies are needed to determine whether such changes perturb aortic wall stress and possibly lead to deleterious long-term effects, such as dilatation of the aortic arch or risk of dissection. Our data indicate that the recent T. David-V-S_{mod} modification of the T. David-V technique reduces helical aortic flow; hence, this operative technique both augments neosinus creation and reduces abnormal changes in distal aortic blood-flow characteristics. The small number of patients with a T. David-V-S_{mod} repair analyzed in this study, however, makes this conclusion conjecture; future studies of more patients are needed.

Valve-sparing aortic root replacement significantly increases late systolic retrograde flow in the distal ascending aorta, and this was more prominent after a T. David-I procedure. Because the patients had no or only mild AR, no correlation between AR and retrograde flow could be established. This retrograde flow may represent energy loss.

Study limitations include the relatively small number of patients and the semiquantitative nature of the data analysis. Because MR velocity-mapping data permits absolute measurements of blood flow velocities, future work should include more quantitative analysis of data from larger patient populations in which vortex formation and helical and retrograde ascending aortic flow are characterized by numeric parameters directly derived from the velocity data. In addition, the temporal and spatial distribution of the velocities could be used to calculate impact forces on the aortic wall and the individual valve cusps themselves, which would help to assess the differences between the various types of David reimplantation procedures and how these might affect long-term valve durability.

The results of the statistical analysis in this study have to be interpreted with caution. Although comparison between all patients (or at least between larger subgroups, such as the combined T. David-V and T. David-V-S_{mod} group) and healthy subjects provided reasonably large numbers, the results associated with smaller sample sizes may be less reliable. Our findings with respect to increased helicity, retrograde flow, and NC cusp vorticity are reliable, but less so for the comparisons between the smaller subgroups.

With respect to data acquisition, future work should be focused on reduction of the total acquisition time and/or improvements in temporal and spatial resolution by using parallel imaging techniques.[27] In addition, optimized respiratory control would improve image quality and reduce blurring, eg, degrading of spatial resolution in the 3D images.

In conclusion, the novel MRI methods presented here should prove to be useful to assess the clinical implications of increased vorticity and altered ascending aortic flow dynamics in patients undergoing various types of valve-sparing aortic root replacements.

ET

References

1. David TE, Feindel CM. An aortic valve-sparing operation for patients with aortic incompetence and aneurysm of the ascending aorta. *J Thorac Cardiovasc Surg.* 1992;103:617-21; discussion 622.
2. David TE, Armstrong S, Ivanov J, Feindel CM, Omran A, Webb G. Results of aortic valve-sparing operations. *J Thorac Cardiovasc Surg.* 2001;122:39-46.
3. de Oliveira NC, David TE, Ivanov J, Armstrong S, Eriksson MJ, Rakowski H, et al. Results of surgery for aortic root aneurysm in patients with Marfan syndrome. *J Thorac Cardiovasc Surg.* 2003;125:789-96.
4. Karck M, Kallenbach K, Hagl C, Rhein C, Leyh R, Haverich A. Aortic root surgery in Marfan syndrome: comparison of aortic valve-sparing reimplantation versus composite grafting. *J Thorac Cardiovasc Surg.* 2004;127:391-8.
5. Miller DC. Valve-sparing aortic root replacement in patients with the Marfan syndrome. *J Thorac Cardiovasc Surg.* 2003;125:773-8.
6. Yun KL, Miller DC, Fann JI, Mitchell RS, Robbins RC, Moore KA, et al. Composite valve graft versus separate aortic valve and ascending aortic replacement: is there still a role for the separate procedure? *Circulation.* 1997;96:II368-75.
7. Bellhouse BJ, Bellhouse FH. Mechanism of closure of the aortic valve. *Nature.* 1968;217:86-7.
8. Leyh RG, Schmidtke C, Sievers HH, Yacoub MH. Opening and closing characteristics of the aortic valve after different types of valve-preserving surgery. *Circulation.* 1999;100:2153-60.
9. Kvitting J-PE, Ebbers T, Wigstrom L, Engvall J, Olin CL, Bolger AF. Flow patterns in the aortic root and aorta studied with time-resolved,

3-dimensional, phase-contrast magnetic resonance imaging: implications for aortic valve-sparing surgery. *J Thorac Cardiovasc Surg.* 2004;127:1602-7.
10. Haacke M, Brown R, Thompson M, Venkatesan R. Magnetic resonance imaging. New York: Wiley-Liss; 1999.
11. Goldin JG, Ratib O, Aberle DR. Contemporary cardiac imaging: an overview. *J Thorac Imaging.* 2000;15:218-29.
12. Firmin DN, Nayler GL, Kilner PJ, Longmore DB. The application of phase shifts in NMR for flow measurement. *Magn Reson Med.* 1990; 14:230-41.
13. Pelc NJ, Herfkens RJ, Shimakawa A, Enzmann DR. Phase contrast cine magnetic resonance imaging. *Magn Reson Q.* 1991;7:229-54.
14. Bogren HG, Buonocore MH. 4D magnetic resonance velocity mapping of blood flow patterns in the aorta in young vs. elderly normal subjects. *J Magn Reson Imaging.* 1999;10:861-9.
15. Wigstrom L, Sjoqvist L, Wranne B. Temporally resolved 3D phase-contrast imaging. *Magn Reson Med.* 1996;36:800-3.
16. Kilner PJ, Yang GZ, Wilkes AJ, Mohiaddin RH, Firmin DN, Yacoub MH. Asymmetric redirection of flow through the heart. *Nature.* 2000; 404:759-61.
17. Fyrenius A, Wigstrom L, Ebbers T, Karlsson M, Engvall J, Bolger AF. Three dimensional flow in the human left atrium. *Heart.* 2001;86:448-55.
18. Kozerke S, Hasenkam JM, Pedersen EM, Boesiger P. Visualization of flow patterns distal to aortic valve prostheses in humans using a fast approach for cine 3D velocity mapping. *J Magn Reson Imaging.* 2001;13:690-8.
19. Kilner PJ, Yang GZ, Mohiaddin RH, Firmin DN, Longmore DB. Helical and retrograde secondary flow patterns in the aortic arch studied by three-directional magnetic resonance velocity mapping. *Circulation.* 1993;88:2235-47.
20. Markl M, Chan FP, Alley MT, Wedding KL, Draney MT, Elkins CJ, et al. Time-resolved three-dimensional phase-contrast MRI. *J Magn Reson Imaging.* 2003;17:499-506.
21. Markl M, Draney MT, Hope MD, Levin JM, Chan FP, Alley MT, et al. Time-resolved 3-dimensional velocity mapping in the thoracic aorta: visualization of 3-directional blood flow patterns in healthy volunteers and patients. *J Comput Assist Tomogr.* 2004;28:459-68.
22. Napel S, Lee DH, Frayne R, Rutt BK. Visualizing three-dimensional flow with simulated streamlines and three-dimensional phase-contrast MR imaging. *J Magn Reson Imaging.* 1992;2:143-53.
23. Mohiaddin RH, Yang GZ, Kilner PJ. Visualization of flow by vector analysis of multidirectional cine MR velocity mapping. *J Comput Assist Tomogr.* 1994;18:383-92.
24. Buonocore MH. Visualizing blood flow patterns using streamlines, arrows, and particle paths. *Magn Reson Med.* 1998;40:210-26.
25. Scheffler K, Lehnhardt S. Principles and applications of balanced SSFP techniques. *Eur Radiol.* 2003;13:2409-18.
26. Walker PG, Cranney GB, Scheidegger MB, Waseleski G, Pohost GM, Yoganathan AP. Semiautomated method for noise reduction and background phase error correction in MR phase velocity data. *J Magn Reson Imaging.* 1993;3:521-30.
27. Pruessmann KP, Weiger M, Scheidegger MB, Boesiger P. SENSE: sensitivity encoding for fast MRI. *Magn Reson Med.* 1999;42:952-62.